

Quantum repeater with Rydberg blocked atomic ensembles in fiber-coupled cavities

E. Brion, F. Carlier, V. M. Akulin
*Laboratoire Aimé Cotton, CNRS / Univ. Paris-Sud / ENS-Cachan,
Bât. 505, Campus d'Orsay, 91405 Orsay, France.*

K. Moelmer
*Lundbeck Foundation Theoretical Center for Quantum System Research,
Department of Physics and Astronomy, University of Aarhus,
Ny Munkegade, Bld. 1520, DK-8000, Aarhus C, Denmark.*

(Dated: July 3, 2018)

We propose and analyze a quantum repeater architecture in which Rydberg blocked atomic ensembles inside optical cavities are linked by optical fibers. Entanglement generation, swapping and purification are achieved through collective laser manipulations of the ensembles and photon transmission. Successful transmission and storage of entanglement are heralded by ionization events rather than by photon detection signal used in previous proposals. We demonstrate how the high charge detection efficiency allows for a shortened average entanglement generation time, and we analyze an implementation of our scheme with ensembles of Cs atoms.

I. INTRODUCTION

A possible route towards scalable quantum computers and quantum communication networks combines small quantum processor nodes which communicate via the exchange of moving information carriers, the so-called *flying qubits*, which will typically be photons. The direct exchange of a photon, either through free space or a fiber, between a pair of nodes does not have unit success probability, and to safely communicate quantum states, one can instead apply entangled state in teleportation protocols [1, 2], where the entanglement of two remote nodes can be achieved, e.g. after multiple attempts until a suitable heralding detection event certifies the establishment of the state. For long distances, photon loss makes the success probability small, and hence the average time needed to establish a state for transmission of a single bit of quantum information very long. This problem, however, can be solved by the quantum repeater setup [3] which divides the transmission path between the nodes into smaller segments with auxiliary nodes over which losses are strongly diminished. The auxiliary nodes are first entangled with their nearest neighbors in a heralded way followed by a succession of local measurements which cause the gradual projection on quantum states with entanglement distributed over longer and longer distances (entanglement swapping). The implementation of this approach is compatible with different physical setups involving atomic ensembles and linear optical operations. The most influential proposal is the so-called DLCZ protocol [4], whose feasibility was experimentally considered in its two-node version in [5].

This manuscript presents a quantum repeater scenario, based on the Rydberg blockade phenomenon. Rydberg blockade refers to the strong dipole-dipole interaction between pairs of highly excited atoms, which after laser excitation of a single atom shifts the resonance condition for all the other atoms and hence blocks further excitation by the laser field. Rydberg blockade forbids the

resonant excitation of more than one Rydberg atom in an atomic mesoscopic sample [6], and has been experimentally observed, e.g., in [7, 8]. In [9] it was proposed to take advantage of Rydberg blockade in quantum information processing, leading to an intensive current field of research [10]. Different theoretical proposals have been recently put forward, which allow to take advantage of the full spectroscopic richness of Rydberg interactions for quantum information purposes [11–13], and a novel framework for quantum information encoding and computing has been proposed [10, 14–16], in which register qubit states are physically implemented by the (symmetric) occupational states $|n_i = 0, 1\rangle$ of internal atomic levels $\{|i\rangle, i = 1, \dots, K\}$ in an ensemble of $N_a (> K)$ identical atoms.

The collective laser manipulation of the system combined with the Rydberg blocking interaction allows one to store and universally process information in the subspace of symmetric ensemble states containing at most one atom in each internal level. The primary advantage of ensembles over single atoms consists in their enhanced coupling to external control fields, which allows for efficient and rapid processing. A secondary practical advantage is that even in a multi-qubit register, one merely needs to address the atoms collectively, contrary to individual-atom encoding of qubits which requires the precise control of each and every single particle in the system.

In the quantum repeater we propose here, the nodes are N identical atomic ensembles, placed in cavities which are linked via optical fibers. The internal structure of the atoms is such that each ensemble $k = 1, \dots, N$ accommodates three logical subnodes, called the left (L_k), the right (R_k), and the auxiliary subnode (A_k) in the following. In the first step of our protocol, we entangle the logical state of the subnode (R_k) in the cavity k with the polarization state of a single photon released in the cavity. This photon is then transmitted to the neighboring cavity where it is absorbed by the left sub-

ode (L_{k+1}) degree of freedom of the atomic ensemble in that cavity, which thus becomes entangled with (R_k). A conditional gate applied to subnodes (L_{k+1}) and (A_{k+1}), followed by appropriate ionization detection is used to ensure that no error occurred during the entanglement generation, in particular that the photon was not lost during the transfer through the fiber between the cavities. If needed, subnodes (R_k, L_{k+1}) are reset so that the entanglement generation operation can be repeated until successful. Once all pairs (R_k, L_{k+1}) have been correctly entangled, entanglement is swapped by ensemble operations on every pair (L_k, R_k). Measurements using Rydberg blockade and ionization detection on all subnodes $\{L_k, R_k, k = 2, \dots, (N-1)\}$ finally heralds the entangled state of the remote pair (R_1, L_N) which can be transformed into any required Bell state by application of a unitary operation on (L_N) prescribed by the results of the measurements. If one of the measurements fails, the procedure must be repeated.

We note that the use of Rydberg blocked ensembles as quantum repeaters has been proposed in [17, 18]. Though related our proposal, however, never makes use of photon detection to generate entanglement between neighbouring nodes, we solely rely on ensemble laser manipulations (including ionizing pulses), ion detection whose efficiency can be made very close to one $\eta_d \sim 1$, and photon transmissions through optical fibers. This allows for a shortened entanglement generation average time whose expression is derived in the Appendix.

The paper is structured as follows. In Sec. II, we present our quantum repeater scheme using Rydberg blockaded ensembles in optical cavities coupled by optical fibers. In Sec. III, we analyze the different steps of our protocol with emphasis on their robustness against errors, and we compute the average duration of our scheme. In Sec. IV, we suggest a physical implementation. In Sec. V, we compare our scheme with other schemes for quantum repeaters, and we conclude in Sec. VI.

II. THE MODEL

Our quantum repeater setup consists of N atomic ensembles placed in cavities which are linked by optical fibers (see Fig. 1a). Neighboring cavities are separated by the distance L_0 .

The atomic level structure is represented in Fig. 1b. All the atoms are initially prepared in the ‘‘reservoir’’ state $|s\rangle$, and the atoms have, in addition, six metastable states denoted by $|0_L\rangle, |1_L\rangle, |0_R\rangle, |1_R\rangle, |0_A\rangle, |1_A\rangle$, three excited states $|\varphi_+\rangle, |\varphi_-\rangle, |\varphi_A\rangle$ and three high-lying Rydberg states $|r_+\rangle, |r_-\rangle, |r_A\rangle$. We assume that the transitions given in Table I can be independently and selectively addressed by appropriately tuned laser beams. In particular, it implies that we can couple pairs of states, $|s\rangle \leftrightarrow |r_{\pm,A}\rangle$, $|0_{L,R}\rangle \leftrightarrow |r_-\rangle$, $|1_{L,R}\rangle \leftrightarrow |r_+\rangle$ and $|0_A\rangle, |1_A\rangle \leftrightarrow |r_A\rangle$ via the intermediate states $|\varphi_+\rangle, |\varphi_-\rangle$ or $|\varphi_A\rangle$.

$ 0, 1_A\rangle \leftrightarrow \varphi_A\rangle$
$ 0_{L,R}\rangle \leftrightarrow \varphi_-\rangle$
$ 1_{L,R}\rangle \leftrightarrow \varphi_+\rangle$
$ s\rangle \xleftrightarrow{\sigma_{\pm}} \varphi_{\pm}\rangle$
$ \varphi_A\rangle \leftrightarrow r_A\rangle$
$ \varphi_{\pm}\rangle \leftrightarrow r_{\pm}\rangle$
$ 0_{L,R,A}\rangle \leftrightarrow 1_{L,R,A}\rangle$

Table I: The transitions required by our protocol.

We further suppose that the atomic samples are small enough to operate in the full Rydberg blockade regime, *i.e.* their size should not exceed a few μm . As a consequence, when driving the transition $|s\rangle \leftrightarrow |r_{\pm,A}\rangle$ on a sample with N_a atoms initially in the state $|s\dots s\rangle$, multiply excited states are out of resonance due to the strong dipole-dipole interaction among Rydberg excited atoms, and the transfer of more than a single atom to the Rydberg state $|r_{\pm,A}\rangle$ is blocked. The fields are applied symmetrically to all atoms in each sample, and they hence excite the symmetric collective state with a single Rydberg excitation, $(|r_k s\dots s\rangle + |s r_k s\dots s\rangle + \dots + |s\dots s r_k\rangle) / \sqrt{N_a}$. The associated coupling strength is easily seen to be magnified by the factor $\sqrt{N_a}$ with respect to the coupling strength of the single atom transition $|s\rangle \leftrightarrow |r_k\rangle$. Applying a π pulse on the collective ensemble transition, followed by the single-particle transition $|r_k\rangle \rightarrow |j\rangle$ ($j = 0_L, 1_L, 0_R, 1_R, 0_A, 1_A$), prepares the sample in a stable symmetric collective state $|N_{0_L}, N_{1_L}, N_{0_R}, N_{1_R}, N_{0_A}, N_{1_A}\rangle$ where the N_j 's denote the populations of the different internal levels, restricted to values 0 and 1. Unitary operations can be applied in the eight-dimensional subspace of collective states, $\{|N_{0_L}, (1 - N_{0_L}), N_{0_R}, (1 - N_{0_R}), N_{0_A}, (1 - N_{0_A})\}$, by simply driving the corresponding single-atom transitions $|0_{L,A,R}\rangle \leftrightarrow |1_{L,A,R}\rangle$ and/or $|0_{L,A,R}\rangle, |1_{L,A,R}\rangle \leftrightarrow |r_{+,-,R}\rangle$, as described in [13, 15]. The collective state pairs $(|0_L\rangle, |1_L\rangle)$, $(|0_R\rangle, |1_R\rangle)$, and $(|0_A\rangle, |1_A\rangle)$ at each repeater node can thus be associated with three qubits, referred to as the left (L), right (R) and auxiliary (A) subnodes, in the following.

We shall use a simplified notation for ensemble states, denoting the collective internal state population as $\bar{0}$ and $\bar{1}$, such that, e.g., $|\bar{0}_L; \bar{1}_R; \bar{1}_A\rangle$ denotes the state $|N_{0_L} = N_{1_R} = N_{1_A} = 1; N_{1_L} = N_{0_R} = N_{0_A} = 0\rangle$, where both the right and the auxiliary subnodes occupy the logic state 1, while the left subnode is in state 0.

It is a further requirement of our protocol that the transitions $|s\rangle \leftrightarrow |\varphi_{\pm}\rangle$ couple non-resonantly to two different modes, \pm , with equal frequency and with detunings Δ_{\pm} with respect to the atomic transitions, but different polarization in the cavity (this will legitimate the assumptions we make below on the fiber transmission/losses). Driving the upper transition $|r_{\pm}\rangle \leftrightarrow |\varphi_{\pm}\rangle$ with a laser field with detuning Δ_{\pm} and Rabi fre-

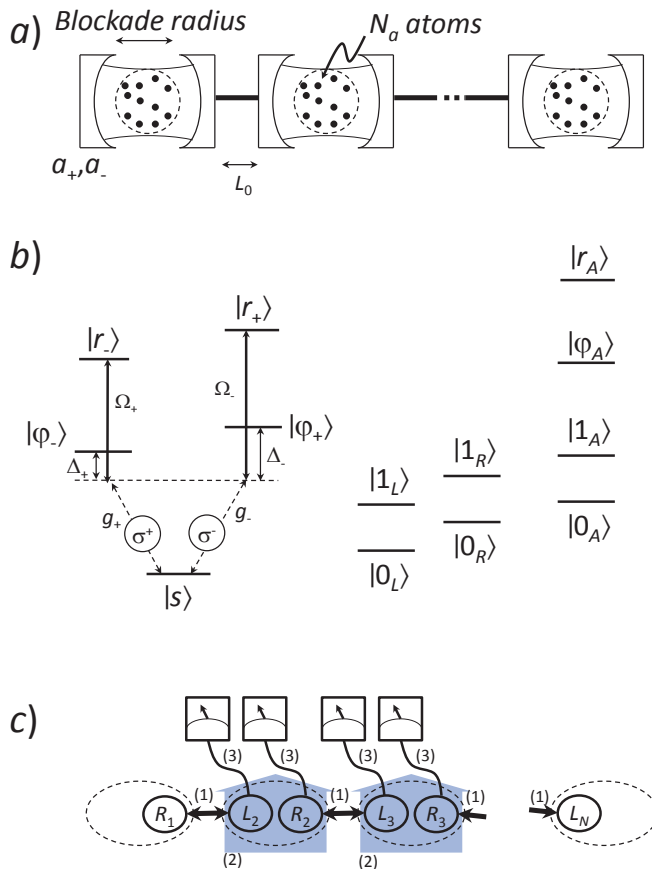


Figure 1: (Color online) a) *The physical set-up for our quantum repeater.* N atomic ensembles are placed in two-mode cavities linked by optical fibers. b) *Atomic level structure.* The figure shows the “quantum-classical” two-photon transitions, $|s\rangle \leftrightarrow |r_\pm\rangle$ driven via the intermediate states $|\varphi_\pm\rangle$ with coupling strength g_\pm to the quantized cavity field modes \pm and with Rabi frequencies Ω_\pm detunings Δ_\pm to the classical laser control fields. c) *The three steps of our scheme.* (1) entanglement of pairs of neighboring subnodes (R_k, L_{k+1}) , entanglement swapping through two-bit gates (2) on each pair (L_k, R_k) and measurement (3) of all subnodes but (R_1, L_N) .

quency Ω_\pm , induces a second-order quantum-classical process, described by the single-atom effective Hamiltonian $\frac{\hbar g_\pm \Omega_\pm}{\Delta_\pm} a_\pm^\dagger |s\rangle \langle r_\pm| + h.c.$ where a_\pm denotes the annihilation operator of the cavity mode \pm and g_\pm its coupling strength. This Hamiltonian derives from the adiabatic elimination of the intermediate state $|\varphi_\pm\rangle$ [19], and is valid for $|\Delta_\pm| \gg |\Omega_\pm|, |g_\pm|$. Performing an ensemble π pulse on the quantum-classical two-photon transition $|s\rangle \leftrightarrow |\varphi_\pm\rangle \leftrightarrow |r_\pm\rangle$ hence converts a collective Rydberg excitation $|r_\pm\rangle$ into a cavity photon \pm and the other way around, with the coupling strength $\hbar\sqrt{N_a}g_\pm\Omega_\pm/\Delta_\pm$. We emphasize that, though only a *single* cavity photon is emitted/absorbed during the process, the coupling can be made strong, thanks to the atomic ensemble magnification factor $\sqrt{N_a}$ [20]. To avoid spurious interference

effects we suggest to apply different detuning parameters for the two transitions proceeding via the same intermediate state $|\varphi_\pm\rangle$.

Optical fibers [21] couple the cavities to each other, and we simply assume that the fiber between two neighboring cavities $(k, k+1)$ achieves the coupling

$$V_{k,k+1} = \sum_{j=0,1} \hbar\alpha_{k,j} [a_{k,j}^\dagger a_{k+1,j} + a_{k,j}^\dagger a_{k+1,j}] \quad (1)$$

with a coupling strength $\alpha_{k,j}$ between the modes $j = +, -$ in the k^{th} cavity with annihilation operator $a_{k,j}$, and the same modes in the $(k+1)^{\text{th}}$ cavity. Since the modes $(+, -)$ differ by their polarizations but have the same frequency, we make the reasonable assumption that the $\alpha_{k,j}$ ’s have the same value α for all (k, j) . We moreover suppose that the coupling between two neighboring cavities can be switched on and off, for instance by a controlled Pockels cell : this will allow us to isolate and separately deal with pairs of coupled nodes.

Due to fiber loss, the transmission of a photon from one cavity to its neighbor is not perfect. We shall assume that the transmission efficiency is the same for all fiber connections and can be written under the form $\eta_t = \exp(-L_0/L_{att})$ where L_{att} is the attenuation length, typically of the order of 22km (corresponding to losses of 0.2dB/km). The probability for losing one photon $(+, -)$ during the transmission along a fiber mode of length L_0 is thus given by $(1 - \eta_t)$.

III. THE SCHEME

In this section, we describe how to entangle two remote nodes using the model we presented in the previous section. First, we briefly sketch the different steps of our scheme in the ideal case without losses. Then, we show how to make our method immune to photon loss and spontaneous emission from the Rydberg level. Finally, we analyze the effects of other possible errors on the performance of our protocol.

A. The different steps of the scheme

Initially, all the cavities are empty and all ensemble atoms are in the reservoir state $|s \dots s\rangle$. The first step consists in entangling pairs of neighboring subnodes (R_k, L_{k+1}) (see Fig. 1c). To this end, one applies the sequence of operations given in Table II. In this table, dashed-line arrows are used for non-resonant couplings to the intermediate states. Moreover, the “ensemble” nature of pulses is emphasized by a $\sqrt{N_a}$ factor above the concerned arrows. Finally, we indicate when a cavity mode is involved in a transition $|s\rangle \leftrightarrow |\varphi_\pm\rangle$ by writing “single photon \pm ” above the corresponding arrow.

<i>i</i>) simultaneous π pulses (same Rabi frequency) on ensemble (k)
$\left\{ \begin{array}{l} s\rangle \xrightarrow{\sqrt{N_a}} \varphi_-\rangle \rightarrow r_-\rangle \\ s\rangle \xrightarrow{\sqrt{N_a}} \varphi_+\rangle \rightarrow r_+\rangle \end{array} \right.$
<i>ii</i>) π pulse on ensemble (k) $ r_-\rangle \xrightarrow{\text{single photon } -, \sqrt{N_a}} \varphi_-\rangle \rightarrow s\rangle$
<i>iii</i>) π pulse on ensemble (k) $ s\rangle \xrightarrow{\sqrt{N_a}} \varphi_-\rangle \rightarrow r_-\rangle$
<i>iv</i>) π pulse on ensemble (k) $ r_+\rangle \xrightarrow{\text{single photon } +, \sqrt{N_a}} \varphi_+\rangle \rightarrow s\rangle$
<i>v</i>) π pulse on ensemble (k) $ s\rangle \xrightarrow{\sqrt{N_a}} \varphi_+\rangle \rightarrow r_+\rangle$
<i>vi</i>) π pulse on ensemble (k) $ r_-\rangle \rightarrow \varphi_-\rangle \rightarrow 0_R\rangle$
<i>vii</i>) π pulse on ensemble (k) $ r_+\rangle \rightarrow \varphi_+\rangle \rightarrow 1_R\rangle$
<i>viii</i>) Transfer of the photon through the fiber from cavity (k) to cavity ($k+1$)
<i>ix</i>) π pulse on ensemble ($k+1$) $ s\rangle \xrightarrow{\text{single photon } -, \sqrt{N_a}} \varphi_-\rangle \rightarrow r_-\rangle$
<i>x</i>) π pulse on ensemble ($k+1$) $ r_-\rangle \rightarrow \varphi_-\rangle \rightarrow 0_L\rangle$
<i>xi</i>) π pulse on ensemble ($k+1$) $ s\rangle \xrightarrow{\text{single photon } +, \sqrt{N_a}} \varphi_+\rangle \rightarrow r_+\rangle$
<i>xii</i>) π pulse on ensemble ($k+1$) $ r_+\rangle \rightarrow \varphi_+\rangle \rightarrow 1_L\rangle$

Table II: The different steps of the entanglement generation procedure.

The first seven pulses (*i* – *vii*) in Table II prepare the subnode (R_k) and the cavity (k) in the entangled state $(|\bar{0}_R\rangle \otimes |-\rangle + |\bar{1}_R\rangle \otimes |+\rangle)/\sqrt{2}$ where $|\pm\rangle$ denotes the number state $|n_{\pm}=1\rangle$ of the cavity mode \pm . The photon thus released is then transferred to the cavity ($k+1$) through the fiber (step *viii*). The last four pulses (*ix* – *xii*) of the sequence translate the photonic excitation into an atomic excitation of the ensemble

($k+1$): a “–” photon is translated into a $|0_L\rangle$ excitation, a “+” photon into a $|1_L\rangle$ excitation. Finally, the two subnodes (R_k, L_{k+1}) are left in the state $(|\bar{0}_R\rangle_k \otimes |\bar{0}_L\rangle_{k+1} + |\bar{1}_R\rangle_k \otimes |\bar{1}_L\rangle_{k+1})/\sqrt{2}$. The sequence of states along which the system evolves during the series of operations described in Table II can be found in Table III.

The entanglement generation procedure described above cannot be applied simultaneously on all pairs (R_k, L_{k+1}): indeed, the pair of nodes to be entangled must be isolated from the others for the photon exchange. One can, however, deal with all the pairs $(R_{2k-1}, L_{2k})_{1 \leq k \leq N/2}$ in parallel. Once entanglement has been successfully established among these pairs, one can then treat the remaining pairs $(R_{2k}, L_{2k+1})_{1 \leq k \leq N/2-1}$. Omitting the auxiliary subnodes and the cavity modes which are all empty, one can write the final state of the system under the form $\prod_{k=1}^{N-1} (|\bar{0}_R\rangle_k \otimes |\bar{0}_L\rangle_{k+1} + |\bar{1}_R\rangle_k \otimes |\bar{1}_L\rangle_{k+1})/\sqrt{2}$.

To complete the scheme, we now need to swap entanglement, *i.e.* to entangle the left and right subnodes (R_k) and (L_k) in every ensemble and decouple the first and last nodes from all the others. This constitutes the second step of the method (see Fig. 1 c). To this end, one first simultaneously applies to each pair of subnodes (R_k, L_k) $_{k=2, \dots, N-1}$ the unitary transformation $(U_L \otimes U_R) \times P_{LR} \times (\mathbb{1}_L \otimes V_R)$, where $U = \exp(-i\frac{\pi}{2}\sigma_z) \times \exp(-i\frac{\pi}{4}\sigma_y)$ and $V = \exp(-i\frac{\pi}{2}\sigma_x) \times \exp(-i\frac{\pi}{2}\sigma_z) \times$

$\exp(-i\frac{\pi}{4}\sigma_y)$ are simply achieved through applying the appropriate laser-induced pulses $|0_{L,R}\rangle \leftrightarrow |1_{L,R}\rangle$ and

$$P_{LR} = \begin{pmatrix} -1 & 0 & 0 & 0 \\ 0 & -1 & 0 & 0 \\ 0 & 0 & 1 & 0 \\ 0 & 0 & 0 & -1 \end{pmatrix} \text{ is implemented through the}$$

following sequence of pulses :

$$\begin{aligned} \pi \text{ pulse : } |0_L\rangle &\rightarrow |r_-\rangle \\ 2\pi \text{ pulse : } |1_R\rangle &\leftrightarrow |r_+\rangle \\ \pi \text{ pulse : } |r_-\rangle &\rightarrow |0_L\rangle. \end{aligned}$$

(Note that all these processes are driven by classical laser beams, via the intermediate states $|\varphi_{\pm}\rangle$.) Finally one measures all subnodes (R_k, L_k) $_{k=2, \dots, N-1}$ through state-selective ionization. This step can be achieved in parallel on the different subnodes. The average time needed for the entanglement swapping operation is hence the time needed for performing the gate and the measurement on a single ensemble.

At the end of the whole procedure, the subnodes (R_1) and (L_N), are decoupled from all the oth-

	$ s \dots s\rangle_k \otimes \text{vac}\rangle_k \otimes s \dots s\rangle_{k+1} \otimes \text{vac}\rangle_{k+1}$	
\xrightarrow{i}	$(N_{r_-} = 1\rangle_k + N_{r_+} = 1\rangle_k) / \sqrt{2} \otimes \text{vac}\rangle_{k+1} \otimes s \dots s\rangle_{k+1} \otimes \text{vac}\rangle_{k+1}$	
\xrightarrow{ii}	$(s \dots s\rangle_k \otimes -\rangle_k + N_{r_+} = 1\rangle_k \otimes \text{vac}\rangle_k) / \sqrt{2} \otimes s \dots s\rangle_{k+1} \otimes \text{vac}\rangle_{k+1}$	
\xrightarrow{iii}	$(N_{r_-} = 1\rangle_k \otimes -\rangle_k + N_{r_+} = 1\rangle_k \otimes \text{vac}\rangle_k) / \sqrt{2} \otimes s \dots s\rangle_{k+1} \otimes \text{vac}\rangle_{k+1}$	
\xrightarrow{iv}	$(N_{r_-} = 1\rangle_k \otimes -\rangle_k + s \dots s\rangle_k \otimes +\rangle_k) / \sqrt{2} \otimes s \dots s\rangle_{k+1} \otimes \text{vac}\rangle_{k+1}$	
\xrightarrow{v}	$(N_{r_-} = 1\rangle_k \otimes -\rangle_k + N_{r_+} = 1\rangle_k \otimes +\rangle_k) / \sqrt{2} \otimes s \dots s\rangle_{k+1} \otimes \text{vac}\rangle_{k+1}$	
\xrightarrow{vi}	$(\bar{0}_R\rangle_k \otimes -\rangle_k + N_{r_+} = 1\rangle_k \otimes +\rangle_k) / \sqrt{2} \otimes s \dots s\rangle_{k+1} \otimes \text{vac}\rangle_{k+1}$	
\xrightarrow{vii}	$(\bar{0}_R\rangle_k \otimes -\rangle_k + \bar{1}_R\rangle_k \otimes +\rangle_k) / \sqrt{2} \otimes s \dots s\rangle_{k+1} \otimes \text{vac}\rangle_{k+1}$	
\xrightarrow{viii}	$ \bar{0}_R\rangle_k \otimes \text{vac}\rangle_k \otimes s \dots s\rangle_{k+1} \otimes -\rangle_{k+1}$ $+ \bar{1}_R\rangle_k \otimes \text{vac}\rangle_k \otimes s \dots s\rangle_{k+1} \otimes +\rangle_{k+1}$	$/\sqrt{2}$
\xrightarrow{ix}	$ \bar{0}_R\rangle_k \otimes \text{vac}\rangle_k \otimes N_{r_-} = 1\rangle_{k+1} \otimes \text{vac}\rangle_{k+1}$ $+ \bar{1}_R\rangle_k \otimes \text{vac}\rangle_k \otimes s \dots s\rangle_{k+1} \otimes +\rangle_{k+1}$	$/\sqrt{2}$
\xrightarrow{x}	$ \bar{0}_R\rangle_k \otimes \text{vac}\rangle_k \otimes \bar{0}_L\rangle_{k+1} \otimes \text{vac}\rangle_{k+1}$ $+ \bar{1}_R\rangle_k \otimes \text{vac}\rangle_k \otimes s \dots s\rangle_{k+1} \otimes +\rangle_{k+1}$	$/\sqrt{2}$
\xrightarrow{xi}	$ \bar{0}_R\rangle_k \otimes \text{vac}\rangle_k \otimes \bar{0}_L\rangle_{k+1} \otimes \text{vac}\rangle_{k+1}$ $+ \bar{1}_R\rangle_k \otimes \text{vac}\rangle_k \otimes N_{r_+} = 1\rangle_{k+1} \otimes \text{vac}\rangle_{k+1}$	$/\sqrt{2}$
\xrightarrow{xii}	$ \bar{0}_R\rangle_k \otimes \text{vac}\rangle_k \otimes \bar{0}_L\rangle_{k+1} \otimes \text{vac}\rangle_{k+1}$ $+ \bar{1}_R\rangle_k \otimes \text{vac}\rangle_k \otimes \bar{1}_L\rangle_{k+1} \otimes \text{vac}\rangle_{k+1}$	$/\sqrt{2}$

Table III: Evolution of the state vector during the entanglement generation procedure.

ers and reduced in one of the four entangled states $\{(|00\rangle \pm |11\rangle) / \sqrt{2}, (|01\rangle \pm |10\rangle) / \sqrt{2}\}$. The unitary W one has to apply on the qubit stored in (L_N) – through driving the appropriate pulse $|0_L\rangle \leftrightarrow |1_L\rangle$, to get the desired state $(|00\rangle + |11\rangle) / \sqrt{2}$ is determined from the outcomes of the measurements : it is indeed obtained as the product of $(N - 2)$ transformations $W = \prod_{k=2}^{N-1} W_k$, where W_k depends on the values $(i_{L_k}, i_{R_k})_{k=2, \dots, (N-1)}$ found for the qubits stored in the left and right subnodes of the ensemble (k) :

$$\begin{aligned}
(i_{L_k}, i_{R_k}) &= (0, 0) \Rightarrow W_k = I \\
(i_{L_k}, i_{R_k}) &= (0, 1) \Rightarrow W_k = \sigma_x \\
(i_{L_k}, i_{R_k}) &= (1, 0) \Rightarrow W_k = \sigma_z \\
(i_{L_k}, i_{R_k}) &= (1, 1) \Rightarrow W_k = \sigma_z \sigma_x
\end{aligned}$$

where $\sigma_x \equiv \begin{pmatrix} 0 & 1 \\ 1 & 0 \end{pmatrix}$ and $\sigma_z \equiv \begin{pmatrix} 1 & 0 \\ 0 & -1 \end{pmatrix}$ are the usual Pauli matrices.

B. Error detection and prevention

So far, we did not take into account errors and losses. Fiber loss and spontaneous emission from the Rydberg level may corrupt the state in quite the same way since they both represent the loss of an excitation. We now investigate the influence of such errors on the different steps of our scheme.

If a photon loss occurs during the transfer through the fiber or if a Rydberg excited atom spontaneously decays

to the reservoir state during one of the steps in Table II, an excitation is missing either in (R_k) or (L_{k+1}) at the end of the entanglement generation procedure. To diagnose whether this is the case, we merely need to test the occupancy of both subspaces $\{|0_R\rangle_k, |1_R\rangle_k\}$ and $\{|0_L\rangle_{k+1}, |1_L\rangle_{k+1}\}$ at the end of the entanglement procedure in the same spirit as in [16]. To this end, one first prepares auxiliary subnodes (A_k) and (A_{k+1}) in the state $|\bar{0}_A\rangle$, before applying to each pair of subnodes (A_k, R_k) and (L_{k+1}, A_{k+1}) the sequence of pulses given in Table IV. At the end of this sequence, the states of the subnodes (R_k) and (L_{k+1}) are unchanged, while the auxiliary subnode (A_k) , respectively (A_{k+1}) , is either in state $|\bar{1}_A\rangle$ if the subnode (R_k) – respectively (L_{k+1}) , is singly occupied, or in the state $|N_{r_A} = 1\rangle$ if the subnode (R_k) – respectively (L_{k+1}) , contains no excitation. One therefore merely needs to selectively ionize $|r_A\rangle$ in both ensembles (k) and $(k + 1)$. *Case (A)* If an ion is observed, subnodes (R_k) and (L_{k+1}) were not correctly entangled, they must therefore be reset through state selective ionization, and the whole procedure in Table II must be repeated. *Case (B)* If no ion is observed then one selectively ionizes the state $|1_A\rangle$ in both ensembles (k) and $(k + 1)$: *Case (B1)* if an ion is observed, as expected, the entanglement generation procedure was indeed correctly performed and the scheme can continue ; *Case (B2)* if no ion is observed, then most probably an ion detection failed and, to be sure, the whole procedure for entangling subnodes (R_k) and (L_{k+1}) must be repeated again, as in the case (A).

In quite the same way, if a Rydberg atom decays during the entanglement swapping procedure, an atomic excitation will miss in one of the subnodes $(R_k, L_k)_{k=2, \dots, N-1}$

and the subsequent series of measurements will therefore fail. In that case, entanglement generation and swapping should be repeated again after resetting the subnodes through state selective ionizations.

As seen above, errors can be detected and their effects avoided through diagnosis and repetition of the erroneous steps. The cost is, however, an increase of the average time required to run the whole protocol, which will now be estimated.

Let us first focus on the entanglement generation procedure. As said in Sec. II, the success probability for a photon transfer along a fiber of length L_0 is $\eta_t = \exp(-L_0/L_{\text{att}})$ where $L_{\text{att}} \sim 22$ km. For $L_0 = 100$ km, $\eta_t \simeq 1.1\%$. On the other hand the probability for one Rydberg excited atom to spontaneously decay during the entanglement generation procedure between two neighboring subnodes (R_k, L_{k+1}) (including the error diagnosis) is roughly given by $n_r \times \frac{\pi}{\Omega} \times \Gamma$ where $n_r = 23$ is the number of (second-order) π pulses involving Rydberg states, Ω is the typical value for their Rabi frequency – note that these pulses can be either “classical-classical” *i.e.* driven by two laser beams or “quantum-classical” *i.e.* they involve a cavity photon in which case the expression of the associated Rabi frequency comprises the coupling strength g_{\pm} , and Γ is the emission rate of the Rydberg level. Taking for the parameters the typical values $\Omega = 2\pi \times 1\text{MHz}$ and $\Gamma = 1\text{kHz}$, one obtains $1 - n_r\pi\Gamma/\Omega \approx 99\%$. Moreover, four ion detections must be successfully performed (giving either a positive or negative result) during the diagnosis on the two subnodes (A_k) and (A_{k+1}) . The probability of this event is given by $\eta_{\text{ion}}^4 \approx 96\%$ for the ion detection efficiency $\eta_{\text{ion}} \approx 99\%$. Finally, the probability for successfully entangling a pair of two neighboring subnodes (R_k, L_{k+1}) is therefore given by $P_0 = \eta_t \times (1 - n_r\pi\Gamma/\Omega) \times \eta_{\text{ion}}^4 \approx 1\%$. Note that the photon transfer is mainly responsible for this low probability, *i.e.* $P_0 \approx \exp(-L_0/L_{\text{att}})$; it is also the longest step of the entanglement generation procedure since it takes $L_0/c = 0.5\text{ms}$ for $L_0 = 100\text{km}$ and $c = 2 \times 10^8\text{m.s}^{-1}$, while each pulse takes no more than $\sim 1\mu\text{s}$, typically, and the duration of an elementary entanglement generation step is roughly given by L_0/c . In average, a pair of neighboring subnodes (R_k, L_{k+1}) will be correctly entangled after $1/P_0$ repetitions of the entanglement generation procedure. For the N -node chain to be correctly entangled, the entanglement generation procedure must be repeated on average a certain number of times $\bar{n}(P_0, N)$, whose expression is calculated in Appendix. For $P_0 \sim 1\%$ and $N = 10$ – *i.e.* for a total length $L \simeq 1000\text{km}$, one obtains $\bar{n}(P_0, N) \simeq 455$.

The same analysis can be achieved for the entanglement swapping step. The success probability of this step is readily found to be $P_1(N) = [(1 - 4\pi\Gamma/\Omega)\eta_{\text{ion}}^4]^{N-2}$. In average, to correctly entangle two remote nodes, $1/P_1(N)$ repetitions of the whole protocol will therefore be necessary. For $N = 10$, $\eta_{\text{ion}} \simeq 99\%$, $\Omega = 2\pi \times 1\text{MHz}$ and $\Gamma = 1\text{kHz}$, one gets $P_1(N) \simeq 71.3\%$.

Finally, since the time necessary for photon transfer,

<i>i</i>) π pulse : $ 1_{L,R}\rangle \leftrightarrow r_+\rangle$
<i>ii</i>) π pulse : $ 0_A\rangle \leftrightarrow r_A\rangle$
<i>iii</i>) π pulse : $ r_A\rangle \leftrightarrow 1_A\rangle$
<i>iv</i>) π pulse : $ r_+\rangle \leftrightarrow 1_{L,R}\rangle$
<i>v</i>) π pulse : $ 0_{L,R}\rangle \leftrightarrow r_-\rangle$
<i>vi</i>) π pulse : $ 0_A\rangle \leftrightarrow r_A\rangle$
<i>vii</i>) π pulse : $ r_A\rangle \leftrightarrow 1_A\rangle$
<i>viii</i>) π pulse : $ r_-\rangle \leftrightarrow 0_{L,R}\rangle$

Table IV: Pulse sequence for diagnosing errors occurring during entanglement generation procedure.

L_0/c , dominates by several orders of magnitude all the other steps, the average time taken by our protocol can be estimated by $T \sim \frac{L_0}{c} \times \frac{\bar{n}(P_0, N)}{P_1(N)}$ that is $T \sim 0.32\text{s}$ for the previous set of parameters, to be compared to the average time it would take via direct transmission through the lossy optical fiber $(1/\chi_r) \times (1/\exp^{-L/L_{\text{att}}}) \sim 5.5 \times 10^9\text{s}$, where χ_r is the repetition rate of the source of photons which we took equal to 10 Ghz for our estimation.

To conclude this section, let us point out that other errors can affect our protocol. First, Rydberg levels can be multiply excited due to the finite value of Δ_{dd} . They constitute losses for our protocol, just as spontaneous emission, and are therefore already dealt with by the scheme.

Their probability is $\left(\frac{\Omega}{\Delta_{dd}}\right)^2 \lesssim 1\%$ and only very weakly modifies P_0 and P_1 .

Secondly, uncertainty in the number of atoms in the sample may lead to inaccuracies in the Rabi frequencies. It was, however, noted in [17], that such errors can be made as low as 1% ; moreover, as suggested in [16], they can also be dealt with by composite pulse techniques. We shall not consider them here.

IV. A PHYSICAL IMPLEMENTATION

In this section, we suggest a physical implementation of our scheme with ensembles of Cs atoms, placed in linear cavities. Fig. 2 presents a possible choice for the internal states used in our protocol. The reservoir state $|s\rangle$ and the subnode states $|0_{L,A,R}\rangle, |1_{L,A,R}\rangle$ correspond to different hyperfine components of the ground level $6s_{1/2}$, $I = 7/2$

$$\begin{aligned}
|s\rangle &\equiv |F = 3; m_F = 0\rangle \\
|0_R\rangle &\equiv |F = 3; m_F = 1\rangle \\
|0_L\rangle &\equiv |F = 4; m_F = -1\rangle \\
|1_R\rangle &\equiv |F = 3; m_F = -1\rangle \\
|1_L\rangle &\equiv |F = 4; m_F = 1\rangle \\
|0_A\rangle &\equiv |F = 3; m_F = 3\rangle \\
|1_A\rangle &\equiv |F = 4; m_F = -3\rangle
\end{aligned}$$

They are coupled to the Rydberg states $|r_{\pm}\rangle = |ns_{1/2}, m_j = \pm 1/2, m_I = \pm 1/2\rangle, |r_A\rangle =$

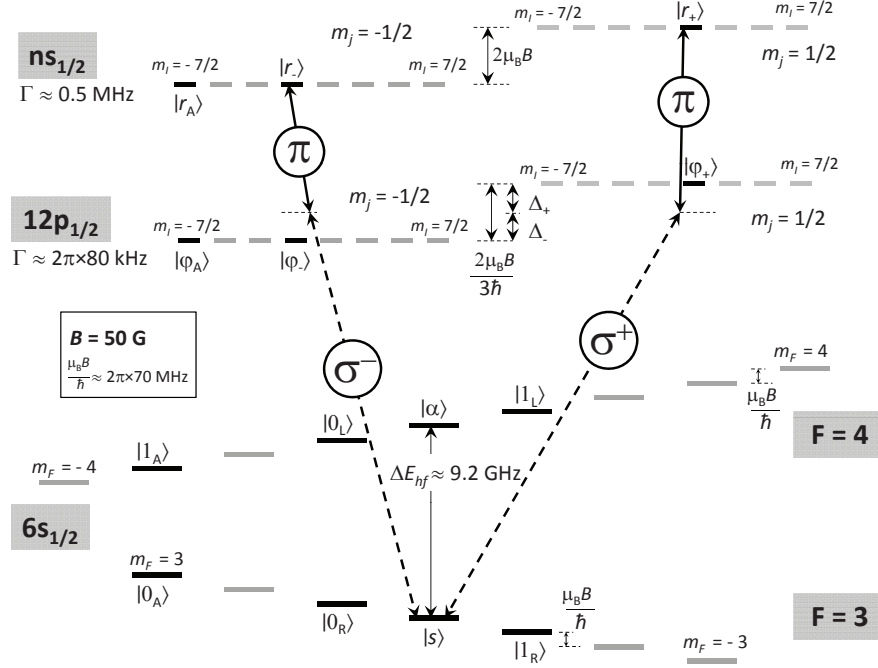


Figure 2: Physical implementation of our scheme with Cs atoms. The figure shows the states $|ji\rangle_{j=0,1;l=L,R,A}, |\varphi_{+,-,A}\rangle$ and $|r_{+,-,A}\rangle$. For sake of clarity, the figure only shows the quantum-classical paths $|r_\pm\rangle \leftrightarrow |\varphi_\pm\rangle \leftrightarrow |s\rangle$ used for converting an atomic excitation into a cavity photon and vice-versa. The dashed-line arrows stand for the transitions driven by the cavity modes \pm , of respective polarizations σ_\pm , the full lines stand for the transitions driven by laser beams of linear polarization. Note that unwanted transitions involving relevant states are out of resonance and therefore highly suppressed.

$|ns_{1/2}, m_j = -1/2, m_I = -7/2\rangle$, with $n \sim 70$, via the intermediate states $|\varphi_\pm\rangle = |12p_{1/2}, m_j = \pm 1/2, m_I = \pm 1/2\rangle$ and $|\varphi_A\rangle = |12p_{1/2}, m_j = -1/2, m_I = -7/2\rangle$. Note that for the intermediate and Rydberg levels, the hyperfine structure may be neglected, which legitimates the use of the decoupled basis. We assume the availability of light sources and cavities at the wavelengths of the required transitions – *i.e.* 335nm and $6.5\mu\text{m}$ for the $6s \leftrightarrow 12p$ and $12p \leftrightarrow 75s$ transitions, respectively [24]. Selection rules show that almost all the transitions necessary to our scheme are *allowed* and that, in particular, the transitions $|\varphi_\pm\rangle \rightarrow |s\rangle$ have different polarizations, that is σ^+ and σ^- , as required (Note that, by setting the quantization axis, *i.e.* the direction of the applied magnetic field, along the axis of the linear cavity, one highly suppresses modes with π polarization). Only the direct coupling $|0_{L,R,A}\rangle \leftrightarrow |1_{L,R,A}\rangle$ is not permitted. To overcome this difficulty, we suggest to resort to intermediate states. To be more explicit, to apply a unitary transformation in the subspace $\{|0_A\rangle, |1_A\rangle\}$ we propose to first transfer the population from $|0_A\rangle$ to $|\varphi_A\rangle$, then to run the desired transformation between $|\varphi_A\rangle$ and $|1_A\rangle$ – which are indeed coupled, and finally transfer the population back from $|\varphi_A\rangle$ to $|0_A\rangle$. The same trick can be used to emulate a coupling between $|0_{R,L}\rangle$ and $|1_{R,L}\rangle$

: one first transfers the population from $|0_{R,L}\rangle$ to $|\varphi_- \rangle$ then to $|\alpha\rangle = |6s_{1/2}; I = 7/2; F = 4; m_F = 0\rangle$ then to $|\varphi_+ \rangle$; one then applies the desired transformation between $|\varphi_+ \rangle$ and $|1_{L,R}\rangle$ before transferring the population back from $|\varphi_+ \rangle$ to $|0_{R,L}\rangle$ along the same path as in the first step.

Moreover, as indicated on Fig. 2, a magnetic field is applied to lift the degeneracies of the different levels. The specific choice we made, that is $B \sim 50$ G, results in splittings of $\frac{\mu_B B}{\hbar} \sim 2\pi \times 17.5$ MHz, $\frac{2\mu_B B}{3\hbar} \sim 2\pi \times 47$ MHz for the hyperfine components $|F = 3, 4; m_F\rangle$ of the ground level and the excited states $|\varphi_\pm\rangle, |r_\pm\rangle$, respectively. These splittings assure that the different transitions required by our protocol are *selectively addressable*, provided that the relevant effective two-photon coupling constant is smaller than $\frac{\mu_B B}{\hbar} \sim 2\pi \times 70$ MHz and respects the finite lifetime of the Rydberg level; moreover, the detunings from the intermediate states $|\varphi_\pm\rangle$ must be chosen larger than $\gamma_{12p} = \tau^{-1} \sim 2\pi \times 80$ kHz, τ being the lifetime of the level $12p_{1/2}$. Typical values of $\Omega \sim 2\pi \times 1$ MHz and $\Delta \sim 2\pi \times 10$ MHz fulfill the previous requirements, and can be achieved for both “classical-classical” and “quantum-classical” paths in a sample of a few hundreds of atoms with $\Omega_{laser} \sim 2\pi \times 1$ MHz and $g_\pm \sim 2\pi \times 0.1$ MHz. Note that the size of the

samples should also be small enough so as to remain in the full blockade regime. As shown in [15], a cloud of $\sim 5\mu\text{m}$ of a few hundreds of atoms, exhibit Rydberg dipole-dipole interactions of at least $\Delta_{dd} \sim 2\pi \times 100\text{MHz}$, which is indeed much larger than Ω and therefore efficiently forbids multiple Rydberg excitations. Finally, all the two-photon processes required in our protocol, including gates on the quantum register, can be performed on the μs timescale. Finally, note that the spontaneous emission from the $12p_{1/2}$ does not constitute a problem when performing unitaries in the subspace $\{|0_A\rangle, |1_A\rangle\}$ through actually populating the state $|\varphi_A\rangle$. Indeed, in this case, we must only fulfill the condition $\Omega_{laser} \ll \frac{\mu_E B}{\hbar} \sim 2\pi \times 70\text{MHz}$ to ensure that no unwanted transition such as $|0_A\rangle \leftrightarrow |12p_{1/2}, m_j = -1/2, m_I = -3/2\rangle$ take place. The frequencies of all the required manipulations – transfers $|0_A\rangle \leftrightarrow |\varphi_A\rangle$ and unitaries $|1_A\rangle \leftrightarrow |\varphi_A\rangle$, can therefore be taken as large as $\sim 2\pi \times 7\text{MHz}$, while the decay rate of the level $12p_{1/2}$ is only $\sim 2\pi \times 80\text{kHz}$: the whole unitary process can therefore be run before the decay of the level $12p_{1/2}$ plays any role.

V. DISCUSSION

We now summarize the main differences between our scheme and the most recent works on the subject [17, 18]. As noted in [17, 18], the use of Rydberg blocked ensembles allows one to perform entanglement swapping via deterministic manipulations and not through probabilistic photonic detections. The main originality of our proposal is that we also completely got rid of photonic detections during the linking procedure. Indeed, here, photons are simply transmitted from one site and reabsorbed by its neighbor in an efficient and faithful way. The heralded linking is performed only via deterministic ensemble manipulations and ion detections, whose efficiency can be made very close to one. In that respect, our scheme is more of a relay type, as defined in [22]. It is also important to note that, contrary to [17], we do not need different ensembles for encoding what we called “subnodes” in the present work, but use the multilevel structure of the atomic spectrum to store three subnodes in the same ensemble. It therefore means that we do not rely on Rydberg blockade between two ensembles, a rather challenging task. We also note that another proposal for a quantum repeater based on atomic ensembles was put forward in [23]. There, however, the authors did not rely on Rydberg blockade phenomenon but rather on fluorescence detection of excitations stored in the atoms after low intensity laser excitation and Raman scattering.

Finally it is worth comparing the total average time needed by our protocol to that required by other schemes, as a figure of merit. Fig. 3 displays the logarithm of the average time necessary for entangling two remote nodes by the direct exchange of a photon – a generous repetition rate of 10 GHz for the photon source was assumed, by the protocol described in [17, 18], and by our protocol

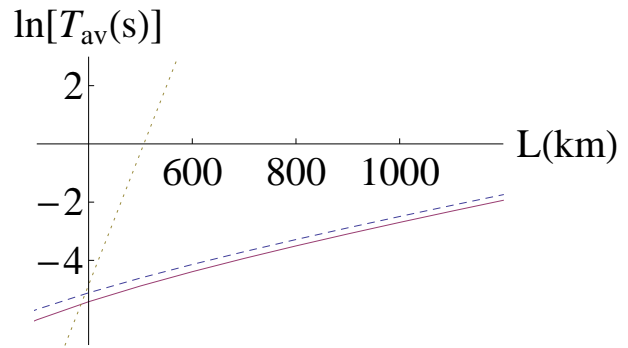


Figure 3: (Color online) Logarithm of the average time required for entangling two remote nodes over the distance L (km), for a total number of nodes $N = 2^4 = 16$, via the direct exchange of a photon (dotted line), through the repeaters described in [10, 18] (dashed line), and through our protocol (full line).

as functions of the distance L between the two nodes to entangle, for a fixed number of $N = 2^4 = 16$ nodes. As in [17, 18], a photodetection efficiency of $\eta_{pd} \simeq 0.9$ and a retrieval efficiency of $\eta_r \simeq 0.9$ (in our cavity model, this retrieval efficiency was taken equal to one) were assumed. It appears that our protocol is quicker, though asymptotically equivalent for $L \rightarrow \infty$, which is explained by our assumption of the ion detection efficiency exceeding that of photons.

VI. CONCLUSION

In this paper we proposed a quantum repeater scenario based on Rydberg blocked ensembles placed in cavities which are linked by optical fibers. Entanglement generation between two neighboring nodes is performed in a heralded way by the transmission of a photon whose polarization is entangled with the state of the first atomic ensemble, followed by its absorption by the neighboring atomic ensemble. Photon losses and spontaneous emission from the Rydberg level can be detected thanks to an error-syndrome measurement involving ensemble laser manipulations, ionizing pulses and (very efficient) ion detections. An implementation with Cs atoms was suggested and analyzed.

Contrary to protocols previously proposed, the scheme presented here does not make use of any (inefficient) photodetection: this potentially allows for a speedup in the entanglement generation, as confirmed by numerical simulations. Finally main error sources were analyzed. Future work should be devoted to a closer investigation of the practical feasibility of our scheme with real cavities and fibers.

Acknowledgments

E. B. thanks M. Raoult, Jean-Louis Le Gouet and F. Prats for fruitful discussions.

Appendix A: Derivation of the expression of the average number of steps in entanglement generation

As described in Sec. III, the entanglement generation procedure is performed in two steps. During each of these steps, $K = N/2$ subnodes are entangled by pairs. A pair of subnodes is correctly entangled with the probability P_0 .

Let us first compute the probability $p_K(n)$ that K pairs are correctly entangled within exactly n repetitions. This means that, within the $(n-1)$ first steps, at least one pair is not entangled. Considering all the possible cases, one establishes the following recurrence formula

$$\begin{aligned} p_K(n) &= p_{K-1}(n)p_1(n) + p_{K-1}(n) \left(\sum_{m=1}^{n-1} p_1(m) \right) \\ &\quad + \left(\sum_{m=1}^{n-1} p_{K-1}(m) \right) p_1(n) \\ &= p_{K-1}(n) \left(\sum_{m=1}^n p_1(m) \right) + \left(\sum_{m=1}^{n-1} p_{K-1}(m) \right) p_1(n) \end{aligned}$$

and, noting that $p_1(n) = P_0(1-P_0)^{n-1}$ one gets

$$p_K(n) = p_{K-1}(n)[1 - (1-P_0)^n] \quad (\text{A1})$$

$$+ \left(\sum_{m=1}^{n-1} p_{K-1}(m) \right) P_0(1-P_0)^{n-1}. \quad (\text{A2})$$

Setting $S_K(n) \equiv \sum_{m=1}^n p_K(m)$, one derives from Eq. (A1) the relation $S_K(n) = S_{K-1}(n)[1 - (1-P_0)^n]$ whence $S_K(n) = S_1(n)[1 - (1-P_0)^n]^{K-1}$ and, since $S_1(n) = [1 - (1-P_0)^n]$, $S_K(n) = [1 - (1-P_0)^n]^K$. One finally deduces the expression for $p_K(n)$ from $p_K(n) = S_K(n) - S_K(n-1)$

$$p_K(n) = [1 - (1-P_0)^n]^K - [1 - (1-P_0)^{n-1}]^K.$$

The average number of repetitions one needs to entangle the K pairs is simply given by $\sum_{n=1}^{+\infty} np_K(n)$.

Since the entanglement of the two groups of $K = N/2$ pairs of subnodes (R_{2k}, L_{2k+1}) and $(R_{2k+1}, L_{2(k+1)})$ is performed independently and successively, the total average number of repetitions required is simply $\bar{n}(P_0, N) = 2 \sum_{n=1}^{+\infty} np_K(n)$ represented on Fig. 4, or, more explicitly

$$\begin{aligned} \bar{n}(P_0, N) &= 2 \sum_{n=1}^{+\infty} n \left\{ [1 - (1-P_0)^n]^K \right. \\ &\quad \left. - [1 - (1-P_0)^{n-1}]^K \right\}. \quad (\text{A3}) \end{aligned}$$

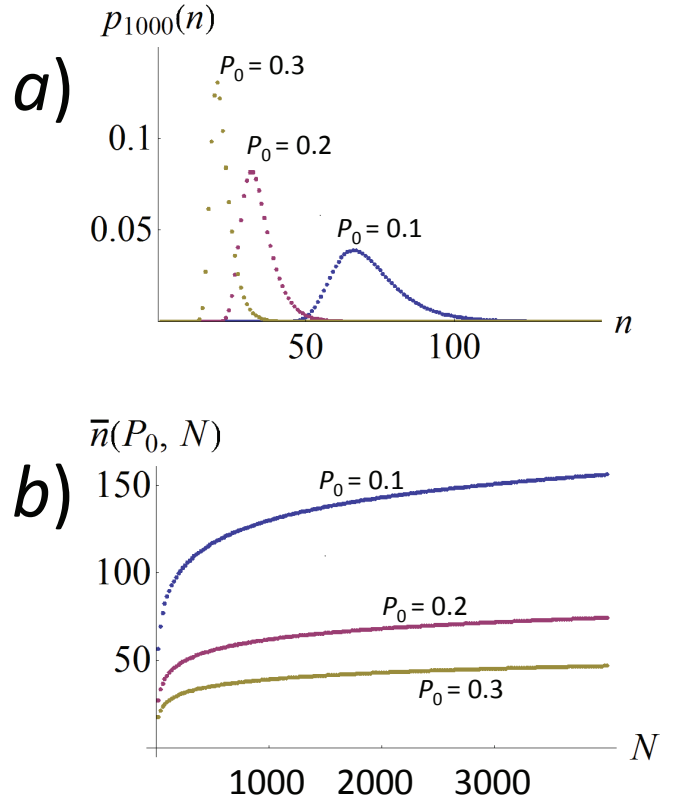


Figure 4: (Color online) a) Generic behaviour of the probability $p_K(n)$ for $K = 1000$ and three different values of $P_0 = 0.1, 0.2, 0.3$. The probability is a peaked curve around its maximum n_K^{max} . b) Behaviour of $\bar{n}(P_0, N)$ as a function of N for three different values of $P_0 = 0.1, 0.2, 0.3$.

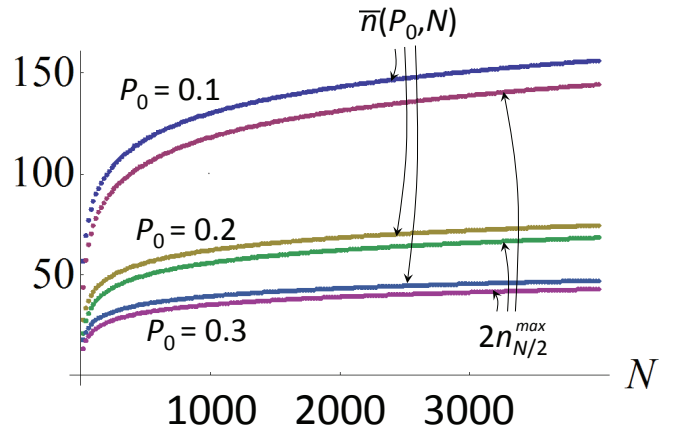


Figure 5: (Color online) Comparison of $\bar{n}(P_0, N)$ and $2n_{N/2}^{max}$ for three different values of $P_0 = 0.1, 0.2, 0.3$.

Let us now derive a simple lower bound for $\bar{n}(P_0, N)$. We shall first note that $p_K(n) = f_K(n) - f_K(n-1)$ where $f_K(n) = [1 - (1 - P_0)^n]^K$; for $n \gg 1$, one thus has $p_K(n) \simeq \frac{df_K}{dn}(n)$ and therefore one can calculate the approximate position of the maximum of $p_K(n)$ by deriving $\frac{df_K}{dn}(n)$. Doing so, one obtains a maximum for $p_K(n)$ at $n = n_K^{max} = -\ln K / \ln(1 - P_0)$. As can be seen on Fig. 4, the distribution $p_K(n)$ is not sym-

metric around its maximum : the position of its peak therefore cannot, strictly speaking, be identified with $\bar{n}(P_0, N = 2K)/2$. It, however, gives a good order of magnitude, $\bar{n}(P_0, N) \gtrsim -2 \ln(N/2) / \ln(1 - P_0)$, as can be checked on Fig. 5. In particular, the expression of $2n_{N/2}^{max}$ gives a good indication on how $\bar{n}(L_0, N)$ scales with the physical parameters.

-
- [1] C. H. Bennett *et al.*, Phys. Rev. Lett. **70**, 1895 (1993).
 [2] C. H. Bennett *et al.*, Phys. Rev. A **54**, 3824 (1996).
 [3] H. J. Briegel, W. Dür, J. I. Cirac and P. Zoller, Phys. Rev. Lett. **81**, 5932 (1998).
 [4] L. M. Duan, M. D. Lukin, J. I. Cirac and P. Zoller, Nature **414**, 413 (2001).
 [5] A. Kuzmich, W. P. Bowen, A. D. Boozer, A. Boca, C. W. Chou, L.-M. Duan, and H. J. Kimble, Nature **423**, 731 (2003).
 [6] D. Comparat and P. Pillet, J. Opt. Soc. Am. B **27**, A208 (2010).
 [7] E. Urban, T. A. Johnson, T. Henage, L. Isenhover, D. D. Yavuz, T. G. Walker, and M. Saffman, Nature Physics **5**, 110 (2009).
 [8] T. Vogt, M. Viteau, J. Zhao, A. Chotia, D. Comparat, and P. Pillet, Phys. Rev. Lett. **97**, 083003 (2006).
 [9] D. Jaksch, J. I. Cirac, P. Zoller, S. L. Rolston, R. Čižek, and M. D. Lukin, Phys. Rev. Lett. **85**, 2208 (2000).
 [10] M. Saffman, T. G. Walker, and K. Mølmer, Rev. Mod. Phys. **82**, 2313 (2010).
 [11] E. Brion, A. S. Mouritzen, and K. Mølmer, Phys. Rev. A **76**, 022334 (2007).
 [12] E. Brion, L. H. Pedersen, K. Mølmer, S. Chutia, and M. Saffman, Phys. Rev. A **75**, 032328 (2007).
 [13] E. Brion, L. H. Pedersen and K. Mølmer, J. Phys. B: At. Mol. Opt. Phys. **40**, S159–S166 (2007).
 [14] M. D. Lukin, M. Fleischhauer, R. Cote, L. M. Duan, D. Jaksch, J. I. Cirac, and P. Zoller, Phys. Rev. Lett. **87**, 037901 (2001).
 [15] E. Brion, K. Mølmer, and M. Saffman, Phys. Rev. Lett. **99**, 260501 (2007).
 [16] E. Brion, L. H. Pedersen, M. Saffman, and K. Mølmer, Phys. Rev. Lett. **100**, 110506 (2008).
 [17] B. Zhao, M. Mølmer, K. Hammerer, and P. Zoller, Phys. Rev. A **81**, 052329 (2010).
 [18] Y. Han, B. He, K. Heshami, C.-Z. Li, and C. Simon, Phys. Rev. A **81**, 052311 (2010).
 [19] E. Brion, L. H. Pedersen and K. Mølmer, J. Phys. A: Math. Theor. **40**, 1033 (2007).
 [20] C. Guerlin, E. Brion, T. Esslinger, and Klaus Mølmer, Phys. Rev. A **82**, 053832 (2010).
 [21] T. Pellizzari, Phys. Rev. Lett. **79**, 5242–5245 (1997).
 [22] N. Sangouard, C. Simon, H. de Riedmatten, and N. Gisin, Rev. Mod. Phys. **83**, 33 (2011).
 [23] J. B. Brask, L. Jiang, A. V. Gorshkov, V. Vuletic, A. S. Sørensen and M. D. Lukin, Phys. Rev. A **81**, 020303 (2010).
 [24] If the $|6s_{1/2}\rangle \leftrightarrow |12p_{1/2}\rangle$ transition is driven via the $|7p_{1/2}\rangle$ state with a classical field at 460nm, the quantum field at the upper transition is at 1.24 μ m which conveniently matches telecommunication fibers.